Effect of Deposition Power on DLC Structure on Alumina in RF-Biased Inductively Coupled Plasma

Zhijun Ai[1], Zhicheng Wu[1], Qiaogen Zhang[1(✉)], Zehao Zhang[1], and Zhengyong Hu[2]

[1] Xi'an Jiaotong University, Xi'an 710049, China
hvzhang@mail.xjtu.edu.cn
[2] State Grid Shanghai Electric Power Company, Shanghai 200125, China

Abstract. Diamond-like carbon (DLC) coating can improve the material surface's friction performance and interfacial compatibility. The current process for DLC deposition on alumina is inadequate, and the effect of deposition power on DLC structure is still unclear. In this paper, the RF-biased inductively coupled plasma (ICP) was introduced to enhance DLC deposition on alumina. By studying the morphology and bonding structure of films under different power conditions, the effects of total power and bias power fraction on DLC structure were decoupled, and the dominant mechanism determining the behavior of the sp^2 phase in the films was investigated. The results show that the increase of total power and bias power fraction led to a decrease in the fraction of sp^3 hybridized carbon in films, and partition phenomena with increasing internal stress. As the total power increased from 90 W to 180 W, the variation trend of sp^2 clusters and CH groups with the bias power fraction reversed, which reflected that the dominant effect factor for deposition changed from implanted ion energy to thermal spike accumulation. The study deepened the understanding of the DLC formation process under plasma action.

Keywords: DLC · Film structure · ICP · PECVD

1 Introduction

Improving the surface properties of alumina by depositing coating is a widely concerned research. Diamond-like carbon (DLC) is an attractive amorphous carbon coating because of its unique surface modification ability in friction, electricity, and biocompatibility [1, 2]. The modification effect is closely linked with the coating structure. For example, the friction properties of the material are related to the DLC morphology and sp^3 sites, and the electrical properties and biocompatibility are determined by the sp^2 sites and CH groups, respectively [3, 4]. Plasma-enhanced chemical vapor deposition (PECVD) provides a wide range of process parameters for DLC deposition, which leads to difficulties in the selection of process parameters for target properties [5]. In RF-biased inductively coupled plasma (ICP), the inductively coupled power and bias power are the

D. Dai et al. (Eds.): ISPEC 2022, SPPHY 391, pp. 44–54, 2023.
https://doi.org/10.1007/978-981-99-1576-7_5

key parameters affecting DLC deposition [6]. This paper aims to clarify the effect of deposition power on DLC structure in RF-biased ICP.

The effect of a single power condition on DLC structure has been extensively studied with silicon as the substrate. Phillips and Thorpe proposed that DLC was a fully constrained random network formed by sp^3 and sp^2 hybridized carbon [7]. The subplantation model by Robertson has explained the phenomenon that the sp^3 fraction first increased and then decreased with increasing bias [3]. The ion energy was considered the key factor for DLC structure in the model and was usually adjusted by a DC bias below substrates. The DC bias caused positive charge accumulation and inhibited film growth, a characteristic that distinguished insulating substrates from doped silicon [8]. To deposit DLC on insulating substrates such as alumina, RF bias was used to neutralize the charge [9]. The bimodal ion energy distribution at RF bias increased the difficulty to adjust film structure, especially when the characteristic time for the ion crossing sheath was much less than the RF period [10].

The ion flux is determined by both inductively coupled power and bias power, while the ion energy is only controlled by the bias condition [11]. To decouple the role of ion flux and energy, we investigated the effect of power conditions with total power and the fraction of bias power as variables. The effects of individual variables on DLC morphology and sp^3 fraction were examined, and the coupling effect of both variables on the behavior of the sp^2 phase and CH groups was further found.

The purpose of this paper is to elucidate the effect of deposition power on DLC structure in RF-biased ICP. The RF-biased ICP enhanced DLC deposition method and the characterization method of DLC structure were described in Sect. 2. The individual effects of total power and bias power fraction on DLC morphology and sp^3 fraction were analyzed in Sect. 3. The coupling effect of power variables on the sp^2 phase and CH groups was found, and the dominant effect mechanism was discussed in Sect. 4. The study deepened the understanding of the DLC formation process under plasma action.

2 Experiments and Methods

2.1 RF-Biased ICP-Enhanced DLC Deposition

An RF-biased ICP-enhanced DLC deposition device was established, as shown in Fig. 1. To increase the nucleation density and deposition rate, high-density ICP was used as the particle source for deposition. RF bias was employed to avoid the inhibition of DLC growth caused by charge accumulation on the highly insulating alumina. The ICP was generated by 40.68 MHz power and the bias condition was adjusted by 13.56 MHz power. Matching networks were connected between power sources and loads for reducing the power reflection. Thanks to the plasma driven by RF power, the electrodes were set outside the reaction chamber to avoid metal contamination. CH_4 passed continuously into the reaction chamber and provided carbon atoms for DLC deposition. The air pressure in the reaction chamber was maintained at 20 Pa by a vacuum pump and measured by a pressure transducer.

It is of primary importance to select the variables of deposition power. The sum of inductively coupled power and bias power ($P_I + P_B$) was used as a variable to describe the ion flux. The fraction of bias power ($P_B/P_I + P_B$) was used as the other variable to

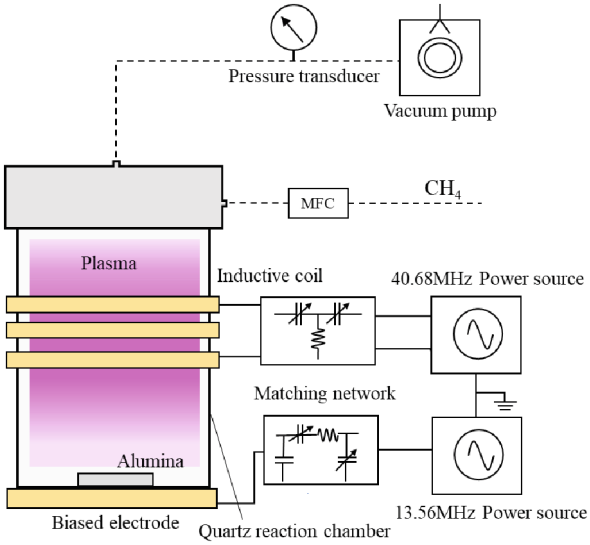

Fig.1. Schematic diagram of RF-biased ICP enhanced DLC deposition device

describe the ion energy. The lower limit of total power is constrained by the deposition threshold, and the upper limit is constrained by the etching effect. The range of total power in experiments was from 90 to 180 W, specifically 90, 120, 150, and 180 W. The bias power fraction included 1/6, 2/6, 3/6, 4/6, and 5/6.

The samples were 2 mm thick alumina discs, which were cleaned with anhydrous ethanol before experiments. In addition, the sample was etched by Ar plasma for 5 min to avoid interference from residual impurities. The deposition process in RF-biased ICP took 10 min.

2.2 DLC Structure Characterization

The morphology and sp^3 fraction were critical to the mechanical properties of films [12]. The microscopic morphology of DLC was observed by field emission scanning electron microscopy (Sigma 300, Carl Zeiss AG, Oberkochen, Germany)). Considering the insulating nature of the samples, the platinum was sputtered on samples before observation. The acceleration voltage was chosen to be 10 kV to avoid excessive charge accumulation. The atomic structure of C was characterized by X-ray photoelectron spectroscopy (ESCALAB Xi+, Thermo Fisher Scientific, Waltham, USA)) and the fraction of sp^3 was obtained by fitting the C1s peak.

The hundreds-fold sensitivity of Raman spectroscopy to sp^2 sites compared to sp^3 sites provides the basis for a more detailed study of sp^2 phase behavior [13]. The Raman spectra were tested by confocal Raman microscopy (LabRAM HR Evolution, Horiba Ltd., Kyoto, Japan) in the range of 800–2000 cm^{-1}, which covered the Raman characteristic of DLC. The laser power was kept below 1.5 mW during tests to avoid sample ablation.

The H bound to C provided the breakpoint for the amorphous carbon network, and the formed CH groups could be characterized by infrared absorption spectroscopy [14]. The infrared absorption spectra of films were tested using an infrared spectrometer (Vertex 70, Bruker Corporation, Billerica, USA). The tests were performed in diffuse reflection mode due to the uneven surface of sintered alumina. The test range was from 2700 to 3200 cm^{-1}, which was the typical absorption band of the CH group.

3 Individual Effects of Power Conditions

3.1 Effect of Total Power

The individual effect of total power on DLC structure was first examined, here focusing on the morphology and sp^3 fraction. The microscopic images of DLC on alumina at different total power are shown in Fig. 2. A large number of submicron particles were observed on the sample without DLC and distributed on the surface or in the interstices of micron particles. The submicron particles were covered by films after DLC deposition and became difficult to be observed with increasing total power. As the total power increased, some wrinkles started to appear in DLC, and divided the film into partitions. The wrinkles were an indication of internal stress release at weak points in films. At 180 W total power, the situation was even more severe, with localized fragmentation in films.

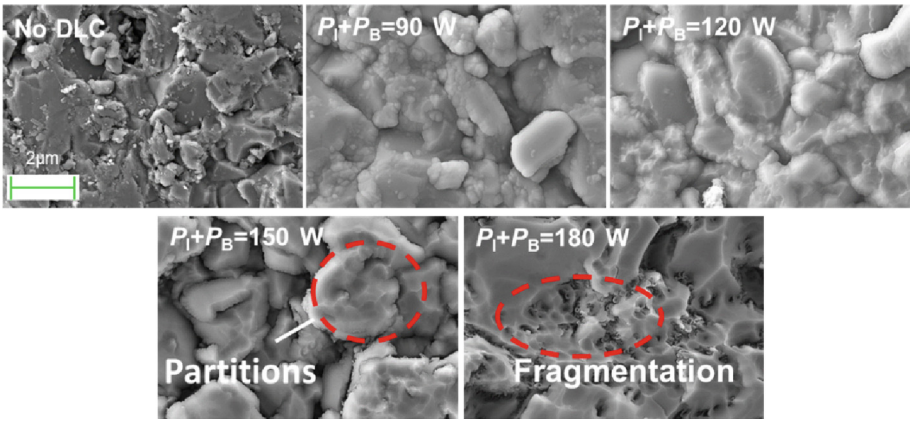

Fig. 2. The microscopic images of DLC on alumina at different total power $P_I + P_B$, bias power fraction $P_B/(P_I + P_B) = 1/6$.

Further attention was paid to the sp^3 fraction, which is directly related to the hardness and density of DLC. The split peak fitting of the C1s peak in X-ray photoelectron spectroscopy (XPS) is shown in Fig. 3a. The peak shapes were assumed to be 80% Gaussian and 20% Lorentzian. The separation of the electron binding energy between the sp^2 peak and sp^3 peak was fixed at 0.5 eV, based on the comparison of C1s and O1s in diamond and graphite [15]. The C1s peak is broadened by the separated peaks, sp^3 and

sp^2, and the full width at half maximum (FWHM) reached 3.0 eV (Fig. 3b). In addition, there is a peak near 286.5 eV corresponding to C-O bonds formed by oxidation of the carbon on the surface. As the total power increased, the FWHM of C1s peak gradually decreased, which implied a possible change in sp^2/sp^3. To quantitatively examine the changing of the sp^3 fraction, we calculated the sp^3 fraction based on the peak area in C1s (Fig. 3b). The results show that the sp^3 fraction decreased from 63.4% to 25.9% as the power increased from 90 W to 180 W.

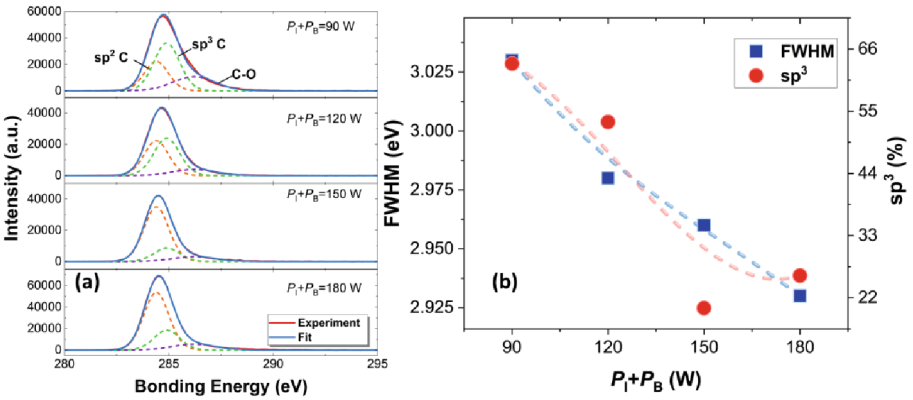

Fig.3. (a)The split peak fitting, (b) FWHM and sp^3 fractions of C1s peaks in XPS at different total power $P_I + P_B$, bias power fraction $P_B/(P_I + P_B) = 1/6$.

3.2 Effect of Bias Power Fraction

The effect of bias power fraction on DLC structure could not be neglected after grasping the effect of total power. The microscopic images of DLC on alumina at different bias power fractions are shown in Fig. 4. At low bias power fraction, the films on different alumina particles were relatively continuous and the film layer could be considered as a single unit. As the bias power fraction increased, the films at gaps were disrupted by high-energy ion bombardment, and the film layer separated. In addition, the partition phenomenon was also observed and intensified with increasing bias power fraction.

To grasp the effect of the bias condition on the sp^3 fraction, the XPS of DLC deposited with different bias power fractions were investigated. The FWHM and sp^3 fractions were obtained by the fitting of C1s peaks in XPS (Fig. 5). The results show that the FWHM decreased with increasing bias power fraction, and the decreasing trend leveled off. At the same time, the sp^3 fraction of DLC decreased from 56.1% to 18.5%, which is similar to that when the total power increased.

3.3 Discussion and Analysis

The increase in total power resulted in more frequent ion bombardment, which can lead to an increase in internal stress in films [16]. The increase of single bombardment

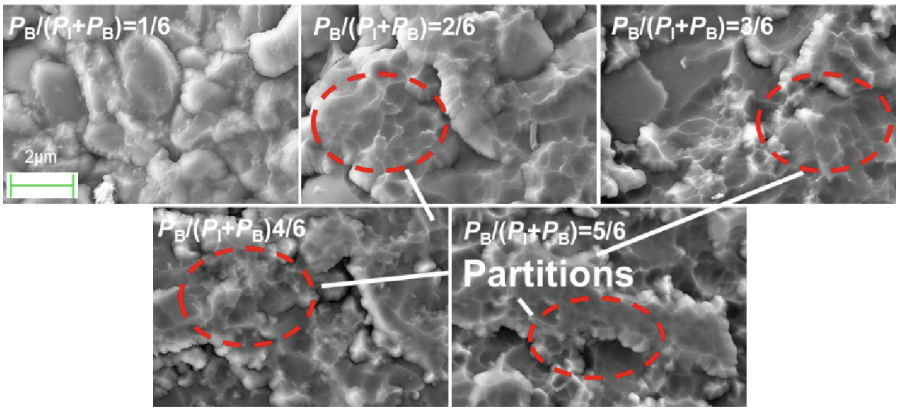

Fig. 4. The microscopic images of DLC on alumina at different bias power fractions $P_B/(P_I + P_B)$, total power $P_I + P_B = 120$ W.

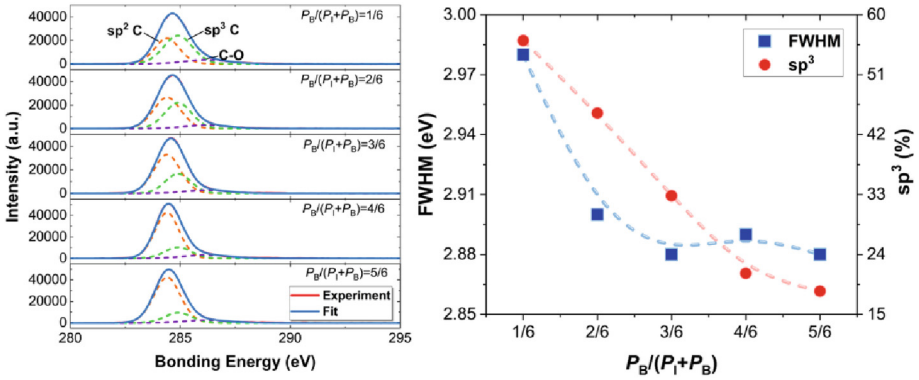

Fig. 5. (a)The split peak fitting, (b) FWHM and sp^3 fractions of C1s peaks in XPS at different bias power fraction $P_B/(P_I + P_B)$, total power $P_I + P_B = 120$ W.

energy with bias condition also contributed to the internal stress [17]. The stress release phenomenon occurred if the internal stress reached a threshold, such as the partitioning of films. The internal stress would be effectively released once the partition occurred.

The formation of the sp^3 site in DLC required a high-pressure environment, which can be provided by internal stresses [18]. The film had a high sp^3 fraction before the stress was released. However, as the internal stress exceeded the threshold and was released, the pressure became unfavorable for the stable presence of the sp^3 site. Therefore, the sp^3 fraction decreased as the total power and bias power fraction increased.

4 Coupling Effect of Power Conditions

4.1 Sp^2 Phase Behavior

The morphology and sp^3 fraction were overall properties of the fully constrained random network and were not sensitive to the differences in effects of total power and bias power fraction [19]. The behavior of the sp^2 phase was studied using Raman spectroscopy to explore the coupling effect between power variables in more detail. The Raman spectrum of DLC has a broad asymmetric peak in the range of 1000 to 1800 cm^{-1} (Fig. 6). The broad peak was composed of D and G peaks, which correspond to the breathing vibration of sp^2 rings and the bond-stretching motion of sp^2 pairs, respectively [20]. A combination of BWF (G peak) and Lorentzian (D peak) line shapes were used to improve the fitting for low-frequency tails. The key characteristic parameters, D and G intensity ratio $I(D)/I(G)$ and G peak position G POS, were used to describe the size of sp^2 clusters and the bond angle disorder of the sp^2 phase, respectively [13].

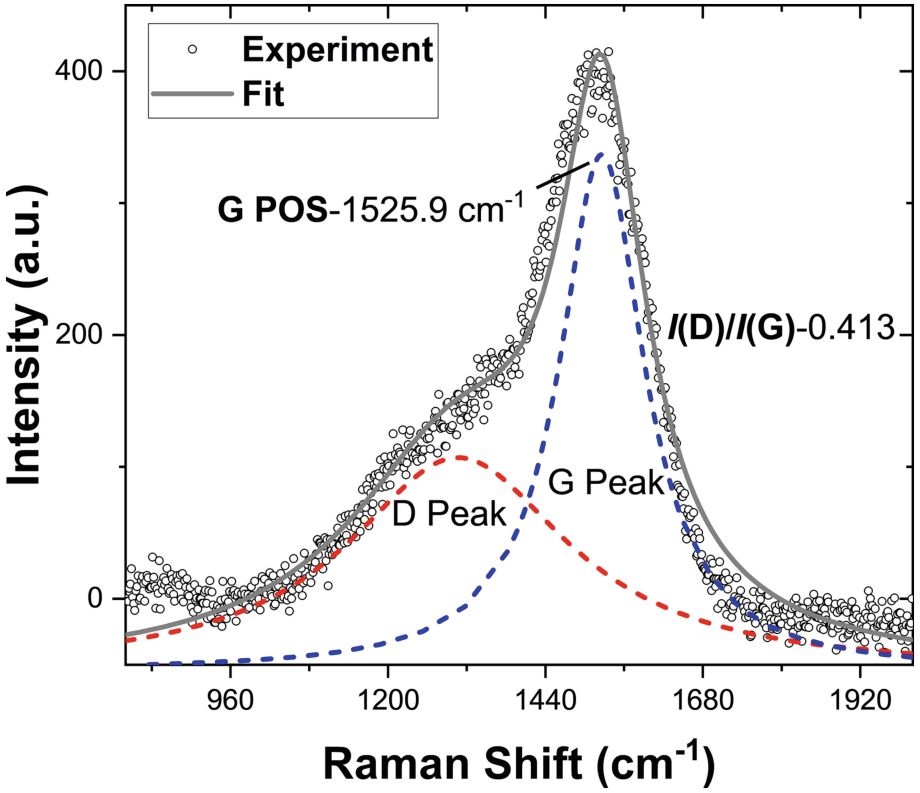

Fig. 6. Typical fitting and characteristic parameters for Raman spectrum of DLC

The Raman characteristics as a function of the bias power fraction at different total power are shown in Fig. 7. At 90 W total power, $I(D)/I(G)$ decreased from 0.40 to

0.33, and G position shifted down from 1530.7 cm^{-1} to 1517.8 cm^{-1} as the bias power fraction increased. The downward shift of the G position implies an increase in the bond angle disorder of the sp^2 phase, and the decrease in $I(D)/I(G)$ implies a decrease in the sp^2 cluster size [21]. At total power above 150 W, the changing trend of Raman characteristics reversed. The bond angle became ordered and the cluster size increased as the bias power fraction increased.

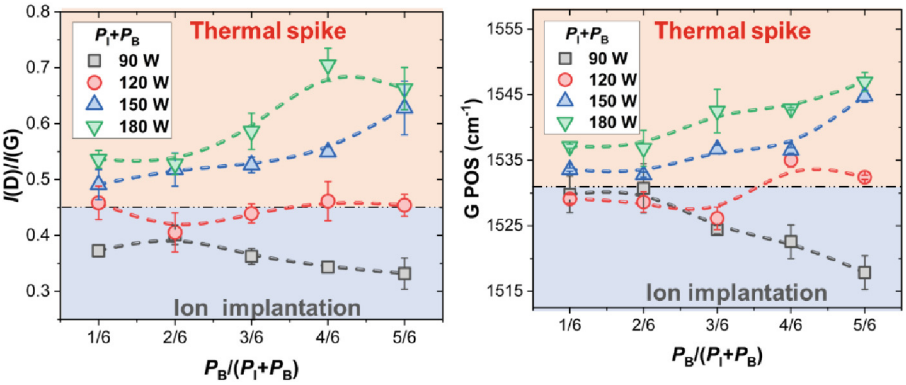

Fig. 7. The Raman characteristics as a function of the bias power fraction $P_B/(P_I + P_B)$ at different total power $P_I + P_B$. The red and blue regions represent the deposition dominant mechanisms are thermal spike accumulation and ion injection, respectively.

The variation in sp^2 phase behavior at different total power showed the coupling effect of power variables. This phenomenon can be explained by the change in the effect mechanism of ion energy on deposition. The ion energy in the deposition area increased with the bias condition [22]. On one hand, the implanted high-energy ions broke the disordered sp^2 rings and reduced the size of sp^2 clusters at low total power. On the other hand, the ion bombardment produced localized thermal spikes, and the relaxation process facilitated sp^2 clustering. As the total power increased, frequent ion bombardment caused severe thermal spike accumulation and the enhancement of sp^2 clustering behavior was observed.

In conclusion, sp^2 clustering was suppressed or enhanced with increasing bias conditions at low and high total power, respectively. The phenomenon was explained by the change of the dominant mechanism from ion implantation to thermal spike accumulation.

4.2 CH Group Behavior

After recognizing the change in the dominant mechanism for DLC deposition, we examined another structure that was sensitive to the action of the thermal spike, CH group. The asymmetric C-H structure was detected by infrared absorption spectroscopy, and typical C-H stretching vibrational modes were in the range of 2800–3100 cm^{-1} [23], as shown in Fig. 8. The absorption peak was divided into two parts, sp^3 CH and sp^2 CH, according to the distribution of vibrational modes. We evaluated the sum and ratio of peak areas, corresponding to the total number of CH groups and the sp^3 CH/sp^2 CH.

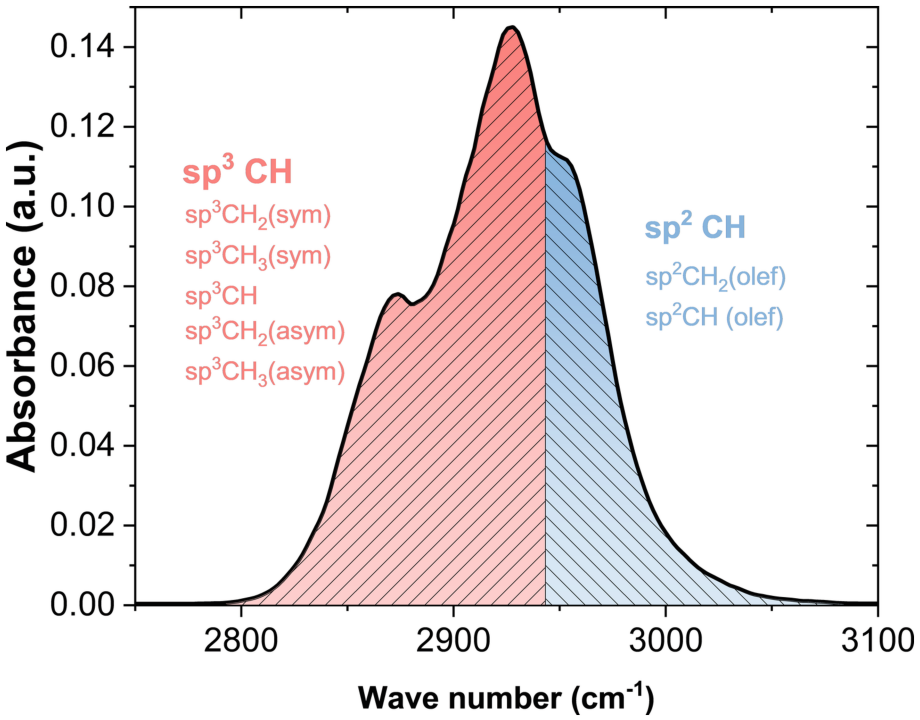

Fig. 8. Infrared absorption spectrum and C-H stretching vibration mode of DLC. (sym-symmetrical, asym-asymmetrical, olef-olefin)

Figure 9 shows the number of CH groups and sp^3 CH/sp^2 CH as a function of bias power fraction at different total power. As the total power increased, the variation

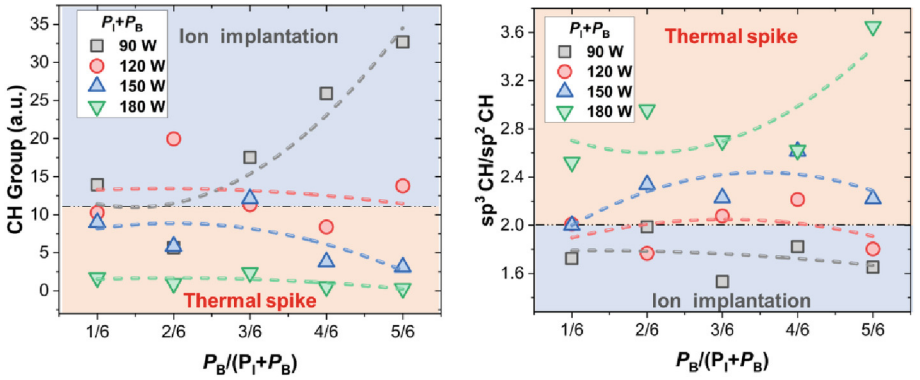

Fig. 9. The number of CH groups and sp^3 CH/sp^2 CH as a function of bias power fraction $P_B/(P_I + P_B)$ at different total power $P_I + P_B$.

law of CH groups on the bias power fraction changed. At low total power, the number of CH groups increased and sp^3 CH/sp^2 CH decreased as the bias power fraction increased. However, at high total power, the total number of CH groups decreased and the sp^3 CH/sp^2 CH increased. This phenomenon was also attributed to the change in the dominant mechanism of DLC deposition.

5 Conclusions

The paper investigates the effect of deposition power on DLC structure on alumina in RF-biased ICP, with total power and bias power fraction as power variables. The conclusions were:

a) At low total power and bias power fraction, alumina particles were covered with continuous films and the sp^3 fraction in DLC reached 63.4%. As the total power or bias power fraction increased, the film wrinkled and partitioned and the sp^3 fraction decreased. The release of internal stress was inferred to be the reason for the reduction of sp^3 phase.
b) The behavior of sp^2 phase and CH groups under different power conditions exhibited the coupling effect of power variables. At 90 W total power, sp^2 phase clustering was suppressed and CH groups and the ratio of sp^2CH increased with the bias power fraction. However, the trends reversed at total power above 150 W. It was attributed to the change in the dominant mechanism from ion implantation to thermal spike accumulation.

Acknowledgement. This work was financially supported by the Science and Technology Project of the State Grid Corporation of China (52094020006W).

References

1. Rajak, D.K., Kumar, A., Behera, A., et al.: Diamond-like carbon (DLC) coatings: classification, properties, and applications. Appl. Sci. **11**(10), 4445 (2021)
2. Erdemir, A., Martin, J.M.: Superior wear resistance of diamond and DLC coatings. Curr. Opin. Solid State Mater. Sci. **22**(6), 243–254 (2018)
3. Robertson, J.: Diamond-like amorphous carbon. Mater. Sci. Eng. R. Rep. **37**(4–6), 129–281 (2002)
4. Castellino, M., Stolojan, V., Virga, A., et al.: Chemico-physical characterisation and in vivo biocompatibility assessment of DLC-coated coronary stents. Anal. Bioanal. Chem. **405**(1), 321–329 (2013)
5. Vetter, J.: 60 years of DLC coatings: historical highlights and technical review of cathodic arc processes to synthesize various DLC types, and their evolution for industrial applications. Surf. Coat. Technol. **257**, 213–240 (2014)
6. Oleszkiewicz, W., Markowski, J., Srnanek, R., et al.: Influence of RF ICP PECVD process parameters of diamond-like carbon films on DC bias and optical emission spectra. Opt. Appl. **43**(1), 109–115 (2013)

7. Phillips, J.C., Thorpe, M.F.: Constraint theory, vector percolation and glass formation. Solid State Commun. **53**(8), 699–702 (1985)
8. Bendavid, A., Martin, P.J., Preston, E.W.: The effect of pulsed direct current substrate bias on the properties of titanium dioxide thin films deposited by filtered cathodic vacuum arc deposition. Thin Solid Films **517**(2), 494–499 (2008)
9. Azhan, N.H., Su, K., Okimura, K., et al.: Radio frequency substrate biasing effects on the insulator-metal transition behavior of reactively sputtered VO2 films on sapphire (001). J. Appl. Phys. **117**(18), 185307 (2015)
10. Cortázar, O.D., Megía-Macías, A.: Bimodal ion energy distribution functions in a hydrogen magnetized plasma. Plasma Sources Sci. Technol. **28**(2), 025010 (2019)
11. Hoekstra, R.J., Kushner, M.J.: Predictions of ion energy distributions and radical fluxes in radio frequency biased inductively coupled plasma etching reactors. J. Appl. Phys. **79**(5), 2275–2286 (1996)
12. Shahsavari, F., Ehteshamzadeh, M., Amin, M.H., et al.: A comparative study of surface morphology, mechanical and tribological properties of DLC films deposited on Cr and Ni nanolayers. Ceram. Int. **46**(4), 5077–5085 (2020)
13. Ferrari, A.C., Robertson, J.: Interpretation of Raman spectra of disordered and amorphous carbon. Phys. Rev. B **61**(20), 14095 (2000)
14. Lemoine, P., Quinn, J.P., Maguire, P.D., McLaughlin, J.A.: Mechanical characterisation and properties of DLC films. In: Donnet, C., Erdemir, A. (eds.) Tribology of Diamond-Like Carbon Films, pp. 83–101. Springer US, Boston, MA (2008). https://doi.org/10.1007/978-0-387-49891-1_3
15. Leung, T.Y., Man, W.F., Lim, P.K., et al.: Determination of the sp3/sp2 ratio of aC: H by XPS and XAES. J. Non-Cryst. Solids **254**(1–3), 156–160 (1999)
16. Aijaz, A., Kubart, T.: Ion induced stress relaxation in dense sputter-deposited DLC thin films. Appl. Phys. Lett. **111**(5), 051902 (2017)
17. Damasceno, J.C., Camargo, S.S., Jr., Freire, F.L., Jr., et al.: Deposition of Si-DLC films with high hardness, low stress and high deposition rates. Surf. Coat. Technol. **133**, 247–252 (2000)
18. Ferrari, A.C., Kleinsorge, B., Morrison, N.A., et al.: Stress reduction and bond stability during thermal annealing of tetrahedral amorphous carbon. J. Appl. Phys. **85**(10), 7191–7197 (1999)
19. Dwivedi, N., Kumar, S., Malik, H.K., et al.: Correlation of sp3 and sp2 fraction of carbon with electrical, optical and nano-mechanical properties of argon-diluted diamond-like carbon films. Appl. Surf. Sci. **257**(15), 6804–6810 (2011)
20. Lubwama, M., Corcoran, B., Rajani, K.V., et al.: Raman analysis of DLC and Si-DLC films deposited on nitrile rubber. Surf. Coat. Technol. **232**, 521–527 (2013)
21. Casiraghi, C., Piazza, F., Ferrari, A.C., et al.: Bonding in hydrogenated diamond-like carbon by Raman spectroscopy. Diam. Relat. Mater. **14**(3–7), 1098–1102 (2005)
22. Gahan, D., Dolinaj, B., Hopkins, M.B.: Retarding field analyzer for ion energy distribution measurements at a radio-frequency biased electrode. Rev. Sci. Instrum. **79**(3), 033502 (2008)
23. Ţucureanu, V., Matei, A., Avram, A.M.: FTIR spectroscopy for carbon family study. Crit. Rev. Anal. Chem. **46**(6), 502–520 (2016)